Integral processing of two-dimensional hyperpolarised ^{13}C-MRS data directly in the time-domain.

D. van Ormondt, R. de Beer
Imaging Physics, TNW
TU Delft, NL

J.W.C. van der Veen
MRS Core Facility
NIMH, NIH
Bethesda, USA

D.M. Sima
ESAT-SCD
KU Leuven, BE

D. Graveron-Demilly
Creatis, Univ Lyon 1
Villeurbanne, FR

***Abstract*—Hyperpolarisation and MRS.**
***Index Terms* — MRS data-processing.**

I. Introduction

In Magnetic Resonance Imaging (MRI) and Magnetic Resonance Spectroscopy (MRS), magnetic nuclei can be oriented either parallel or anti-parallel to the strong applied static magnetic field B_0. At body temperature, $T \approx 310$ K, these two alternative states are nearly equally populated, according to the so-called Boltzmann distribution at thermal equilibrium [1]. The difference in population of the two states defines the nuclear magnetic *polarisation*. When they are equally populated, the polarisation is 0; when only one state is populated, it is $\pm$ 1.

The natural nuclear magnetic polarisation of a patient in a scanner is very low, namely of the order of 10^{-5} [1]. The magnitude an MR-signal being proportional to the polarisation, it follows that the signal-to-noise ratio (SNR) of MRI and MRS is far from optimal.

Under the circumstance, clinics may have to turn to the more sensitive *in vitro* techniques, based on body fluids, *i.e.*, urine, blood, etc. Such techniques are available and widely applied [2,3]. However, being *in vitro* they cannot provide information about the original location of molecules of interest inside a patient.[1]

Alternatively, clinics can resort to so-called 'hyperpolarisers' (HP[2]) which are capable of raising nuclear magnetic polarisation by, *e.g.*, four orders of magnitude above the value at thermal equilibrium [4]. The SNR benefits by the same amount. Promising results keep coming; see, *e.g.*, Refs. [5,6,7,8,9,10,11,12,13].

Despite progress, a point of concern is that preparing HP of nuclei is to be carried out *outside* a patient, for practical reasons. Once sufficient HP has been attained, the molecules hosting the polarised nuclei are to be injected into a patient. This has to be done with minimal time delay because return to low SNR takes place in about 2 minutes[3]. Such a limited time slot requires hasty measurements resulting in sparse data-aquisition, possibly with 'missing' data-points, which in turn requires non-conventional data-processing. Fig. 1 shows an example of evolving metabolite concentrations during and after injection of HP-pyruvate.

The present paper pertains to HP-MRS data-processing of measurements simulated from physical-chemical information provided in Refs. [5,6].

Before proceeding, we mention for non-experts that HP-MRS measurements are two-dimensional, *i.e.*, there are two time-dimensions, with running variables t^{HP} and t^{MRS}, and aquisition (sample) times t_n^{HP}, $n = 1, 2, \ldots, N^{\text{HP}}$ and $t_{n'}^{\text{MRS}}$, $n' = 1, 2, \ldots, N^{\text{MRS}}$, respectively. In both dimensions, signals have a characteristic decay time, namely τ^{HP} and τ^{MRS}[4]. A mathematically convenient physical condition is that $\tau^{\text{MRS}} \ll \tau^{\text{HP}}$. As a consequence, one may assume that HP-decay takes place only in between successive acquisitions of an MRS-signal.

Here, we distinguish two main ways of data-processing:

- *Traditional, two-step data-processing*

In Refs. [5,6], the data in the two dimensions are traditionally processed separately, in two steps:

1) First, one estimates the evolving concentrations of the metabolite species of interest from each of the N^{HP} consecutive one-dimensional MRS-signals, acquired at times $t_{n'}^{\text{MRS}}$, $n' = 1, 2, \ldots, N^{\text{MRS}}$, separately. See an example of evolving concentrations, also indicated by HP-evolution, in Fig. 1.
2) Second, one fits chemical exchange formula's to the set of one-dimensional curves estimated for times t_n^{HP}, $n = 1, 2, \ldots, N^{\text{HP}}$ of step 1.

- *Alternative, single-step data-processing*

Deviating from tradition, we here fit a joint, two-dimensional model function to all acquired HP-MRS data simultaneously. To this end the $N^{\text{HP}} \times N^{\text{MRS}}$ samples are merged into a single, large, one-dimensional array (vector). We introduced this approach previously, for processing so-called inversion-recovery data [14], but to the best of our knowledge, it is new for HP-MRS data. Fitting all data simulaneously needs rather fewer free model parameters. As a consequence, its execution should be less cumbersome and result in reduction of estimation errors.

[1] Note that MRI and MRS operate *in vivo*, non-invasively, and do reveal the locations of molecules of interest within a patient.

[2] In the sequel, the abbreviation HP stands for *hyperpolarisation* or *hyperpolarised*, depending on the context.

[3] But see Refs. [12,13]

[4] Both τ^{HP} and τ^{MRS} are metabolite species-dependent. For the sake of simplicity we do not adhere to the usual magnetic resonance symbols.

The sequel is devoted to **Methods** (Sec. II), **Results** (Sec. III), **Discussion** (Sec. IV), **Concluding Remarks** (Sec. V).

II. METHODS

A. Preamble

We simulated the HP-MRS data with the model function [6,15]

$$s(t_n^{\rm HP}, t_{n'}^{\rm MRS}) = \sum_{m=1}^{M} \left[\overbrace{\psi_m(t_n^{\rm HP})}^{\text{evolving HP}} \; \overbrace{f_m(t_{n'}^{\rm MRS})}^{\text{MRS signal}} \right], \quad (1)$$

in which the running times $t_n^{\rm HP}$, $n = 1, \ldots, N^{\rm HP}$, and $t_{n'}^{\rm MRS}$, $n' = 1, \ldots, N^{\rm MRS}$, were defined above in Sec. I. The values of m relate to the metabolite species involved. The left-hand term of the product contained in the square brackets represents the time-dependent (evolving) concentration of HP metabolite species m; the right-hand term represents the related MRS-signals of HP metabolite species m, per unit of concentration.

B. HP-evolution model function ψ_m in Eq. 1

The metabolite species of interest in this work are pyruvate (Pyr), lactate (Lac), alanine (Ala), bicarbonate (BC) [5,6], here numbered $m = 1, 2, 3, 4$ respectively. See Fig. 1. Pyr is injected from $t_{\rm a} = 2$ s till $t_{\rm e} = 12$ s, the subscripts $_{\rm a}$ and $_{\rm e}$ standing for arrival and end respectively. For $t < t_{\rm a}$, the concentrations are too low to be detectable by MRS. For $t_{\rm a} < t < t_{\rm e}$, the concentrations of all metabolites increase, that of Pyr injected at constant rate I up to a maximum at $t = t_{\rm e}$, while those of Lac, Ala, BC peak somewhat later. The MRS-signals are proportional with these concentrations; see example in Fig. 2.

Adapting the symbols in Eqs. (8,10) of Ref. [6] to those used above, the model functions ψ_m which govern the evolving concentrations of the four HP-metabolite species are

For $t_{\rm a} < t < t_{\rm e}$ and $m = 1$:

$$\psi_1(t) = I\,\tau_1^{\rm HP}\left[1 - e^{(t-t_{\rm a})/\tau_1^{\rm HP}}\right], \quad (2)$$

for $t \geq t_{\rm e}$ and $m = 1$:

$$\psi_1(t) = \psi_1(t_{\rm e})\, e^{(t-t_{\rm e})/\tau_1^{\rm HP}}, \quad (3)$$

for $t_{\rm a} < t < t_{\rm e}$ and $m = 2, 3, 4$:

$$\psi_m(t) = I\,k_m^1\,\frac{\tau_m^{\rm HP}\,\tau_1^{\rm HP}}{\tau_m^{\rm HP} - \tau_1^{\rm HP}}\left[\frac{(1 - e^{(t-t_{\rm a})/\tau_m^{\rm HP}})\,\tau_m^{\rm HP}}{(1 - e^{(t-t_{\rm a})/\tau_1^{\rm HP}})\,\tau_1^{\rm HP}}\right], \quad (4)$$

for $t \geq t_{\rm e}$ and $m = 2, 3, 4$:

$$\psi_m(t) = \psi_1(t_{\rm e})\,k_m^1\,\frac{\tau_m^{\rm HP}\,\tau_1^{\rm HP}}{\tau_m^{\rm HP} - \tau_1^{\rm HP}}\left[e^{(t-t_{\rm e})/\tau_m^{\rm HP}} - e^{(t-t_{\rm e})/\tau_1^{\rm HP}}\right] + \psi_m(t_{\rm e})\, e^{(t-t_{\rm e})/\tau_m^{\rm HP}}, \quad (5)$$

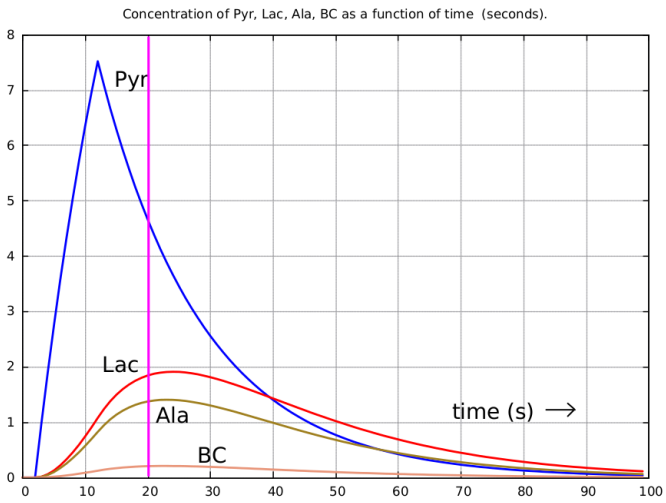

Figure 1. Evolution of the concentrations of metabolite species pyruvate (Pyr, $m = 1$), lactate (Lac, $m = 2$), alanine (Ala, $m = 3$), bicarbonate (BC, $m = 4$), as a function of $t^{\rm HP}$, simulated with Eqs. (2,3,4,5). The magenta line marks the time at which the data for Fig. 2 were acquired.

where k_m^1 is the exchange rate from metabolite species 1 to metabolite species $m = 2, 3, 4$. The meaning of the other symbols in Eqs. (2,3,4,5) was given above, in Subsec. II-B.

C. MRS-signal model function f_m in Eq. 1

If the concentration of a metabolite species m equals c_m, the attendant one-dimensional MRS-signal is [16,17]

$$c_m\, f_m(t) = c_m\, e^{i\varphi_0}\, e^{-(t/\tau_m^{\rm MRS}) + i\,2\pi\nu_m t}, \quad (6)$$

where $i = \sqrt{(-1)}$, φ_0 is a phase, and ν_m is the precession frequency of the HP-nuclei involved. In the two-dimensional HP-MRS experiments, the normally constant concentration c_m is replaced by the time-dependent entity ψ_m, as already pointed out in Subsec. II-A.

For the sake of simplicity, we assumed simple exponentional decay with time constant $\tau_m^{\rm MRS}$. Usually, more elaborate decay functions occur in *in vivo* MRS [15] but this aspect is less important in the context of testing two-dimensional fitting.

D. Fitting of Eq. 1 to all data in a single step

As mentioned in Sec. I, a two-dimensional HP-MRS measurement entails $N^{\text{HP-MRS}} = N^{\rm HP} \times N^{\rm MRS}$ samples. For the purpose of processing, we group these samples into a one-dimensional array (vector)[5], $\overline{\text{data}}$, of size $N^{\text{HP-MRS}}$. Surrogate data were calculated from Eq. (1) by substituting parameter values, $p_\ell, \ell = 1, \ldots, L$, gleaned from Ref's [5,6] and adding white Gaussian noise with standard deviation $\sigma_{\rm noise}$. The chosen set of parameters is grouped into a vector $\overline{p}_{\rm true}$. In addition, we introduce a noiseless vector $\overline{\text{calc}}$, also calculated from Eq. (1), but with free parameter values grouped into $\overline{p}_{\rm fit}$. Defining further

[5] We denote a vector, or one-dimensional array, by a bar above the symbol in question.

$$J((n-1)N^{\text{MRS}}+n',\ell) \stackrel{\text{def}}{=} \frac{\partial s(t_n^{\text{HP}}, t_{n'}^{\text{MRS}})}{\partial p_\ell}, \quad (7)$$

$$\Delta\overline{p} \stackrel{\text{def}}{=} \overline{p}_{\text{fit}} - \overline{p}_{\text{true}}, \quad (8)$$

$$\overline{\text{residu}} \stackrel{\text{def}}{=} \overline{\text{model}} - \overline{\text{data}}, \quad (9)$$

in which J, the 'Jacobian' (Appendix 1), is a two-dimensional array with $N^{\text{HP}} \times N^{\text{MRS}}$ rows and L columns, we write

$$\Delta\,\overline{\text{model}} = J\,\Delta\overline{p} \approx \overline{\text{residu}}, \quad (10)$$

in which the left-hand side equals the first order change of the model of Eq. (1) when the model parameters $\overline{p}_{\text{fit}}$ are varied by a small amount $\Delta\overline{p}$. Analytic expressions of the partial derivatives in Eq. (7) were obtained from the free computer algebra package wxMaxima.

Starting with $\overline{p}_{\text{fit}} = \overline{p}_{\text{start}}$, Eq. (10) was solved iteratively with subroutine DGELSS of the free linear algebra package LAPACK, using modern FORTRAN, *i.e.*, GNU f95, which in addition contains features of f2003/f2008. In essence, this amounts to the Gauss-Newton variant of non-linear least-squares (NLLS) fitting. The stop-criterion of the iterations was that $\sum_{l=1}^{L} |\Delta p_{\text{fit},\ell}|$ be smaller than δ, where δ is a small number the size of which depends on the level of the noise. On average, 11 iterations were needed with the noise level corresponding to the upper spectrum in Fig. 2.

Finally, we mention that Ref. [6] estimates either t_{a} or t_{e}, given that the difference between the two equals 10 s. The partial derivatives w.r.t. these parameters being discontinuous, we have estimated t_{e} separately from the position of the sharp maximum of ψ_1 (1 = Pyr) visible in Fig. 1. This issue will be a subject of later investigation, after gaining insight in details of the evolution of Pyr around the end of its injection. For the time being, this results in $L = 17$.

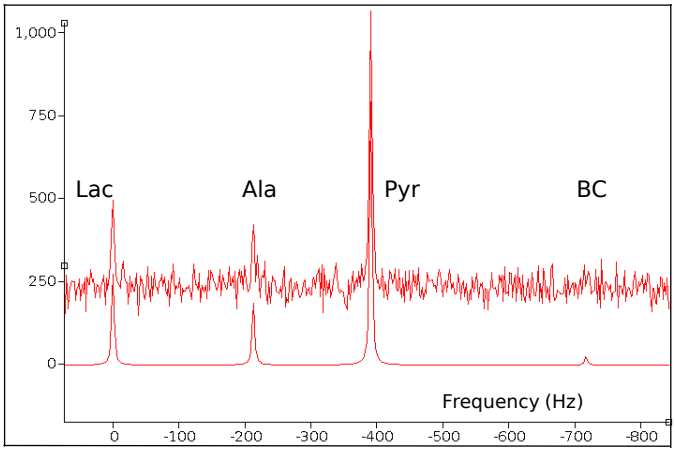

Figure 2. Re[FFT($s(t^{\text{HP}} = 20, t^{\text{MRS}})$)] of the simulated signal for $\sigma_{\text{noise}} = 0$ and 1.0. See Fig. 1 at $t^{\text{HP}} = 20$ s. Graph made with the free software package jMRUI [18].

E. Errors of estimation

We obtained the errors in the estimated model parameters from a Monte Carlo procedure with thousand different realisations of white Gaussian noise with equal standard deviation, σ_{noise}. This required calling subroutine c8_normal_01(seed,cnoise).f90 [6] 2048×10^5 times. Each realisation yields a different set of estimated model parameters. From the latter, we obtained the means and standard deviations of the estimates.

An important test of the Monte Carlo procedure is whether the differences between mean and true values (= bias) are small with respect to the standard deviations, and whether the standard deviations approach the Cramér Rao bounds (CRB's). Our CRB's are based on the theory in Ref. [19], and use of Eqs. (1-6,11) and $\overline{p}_{\text{true}}$ for computing numerical values of the elements of J; see results in Table I.

Table I
CRB'S AND CORRESPONDING STANDARD DEVIATIONS, σ_{MC}, OF **ERRORS** IN PARAMETERS, ESTIMATED IN A MONTE CARLO (MC) EXPERIMENT. THE ATTENDANT SIMULATED DATA WERE CORRUPTED WITH NOISE WITH STANDARD DEVIATION $\sigma_{\text{NOISE}} = 0.01, 1.0$. THE CHEMICAL EXCHANGE FROM METABOLITE 1 TO METABOLITE m IS INDICATED BY $k_m^1, m = 2, 3, 4$; SEE EQS. (4,5).
1 = PYR, 2 = LAC, 3 = ALA, 4 = BC.

Case → Param.↓	CRB $\div\ \sigma_{\text{noise}}$	σ_{MC} for $\sigma_{\text{noise}} = 0.01$	σ_{MC} for $\sigma_{\text{noise}} = 1.0$
Inject	0.770×10^{-2}	0.762×10^{-4}	0.762×10^{-2}
k_2^1	0.834×10^{-3}	0.850×10^{-5}	0.853×10^{-3}
k_3^1	0.957×10^{-3}	0.970×10^{-5}	0.971×10^{-3}
k_4^1	1.000×10^{-3}	0.971×10^{-3}	1.110×10^{-3}
$1/\tau_1^{\text{HP}}$	0.508×10^{-3}	0.504×10^{-5}	0.504×10^{-3}
$1/\tau_2^{\text{HP}}$	0.158×10^{-2}	0.168×10^{-4}	0.169×10^{-2}
$1/\tau_3^{\text{HP}}$	0.266×10^{-2}	0.273×10^{-4}	0.274×10^{-2}
$1/\tau_4^{\text{HP}}$	0.192×10^{-1}	0.191×10^{-3}	0.228×10^{-1}
φ_0	0.528×10^{-2}	0.508×10^{-4}	0.507×10^{-2}
$1/\tau_1^{\text{MRS}}$	0.499×10^{-4}	0.499×10^{-6}	0.500×10^{-4}
$1/\tau_2^{\text{MRS}}$	0.143×10^{-3}	0.140×10^{-5}	0.140×10^{-3}
$1/\tau_3^{\text{MRS}}$	0.228×10^{-3}	0.223×10^{-5}	0.224×10^{-5}
$1/\tau_4^{\text{MRS}}$	0.173×10^{-2}	0.174×10^{-4}	0.201×10^{-2}
ν_1	0.756×10^{-5}	0.721×10^{-7}	0.720×10^{-5}
ν_2	0.171×10^{-4}	0.174×10^{-6}	0.174×10^{-4}
ν_3	0.264×10^{-4}	0.269×10^{-6}	0.269×10^{-4}
ν_4	0.196×10^{-3}	0.198×10^{-5}	0.211×10^{-3}

[6] See J. Burkardt. Actually, in the repository, the subroutine is a function.

$$\mathrm{CRB}_\ell = \sigma_{\mathrm{noise}} \sqrt{[(J^{\mathrm{T}}J)^{-1}]_{\ell,\ell}}\,, \ell = 1, \ldots, L\,. \quad (11)$$

III. Results

Table I lists the standard deviations σ_{MC} of the $L = 17$ estimated parameters, as obtained from the Monte Carlo experiment. Also listed are the corresponding CRB's to compare with. In accordance with theory, the CRB's approach the standard deviations σ_{MC}, obtained from the Monte-Carlo procedure very well. Naturally, the agreement is better for $\sigma_{\mathrm{noise}} = 0.01$ than for $\sigma_{\mathrm{noise}} = 1.0$. As was to be expected, the agreements turned out to be least good for metabolite species BC ($m = 4$), which has the lowest concentration.
Another notable result of the Monte Carlo experiment, shown in Table II in the Appendix, is that $\mathrm{bias}_{\mathrm{MC}} \ll \sigma_{\mathrm{MC}}$, especially for the most concentrated metabolite species. Apparently, the estimator is still above threshold at $\sigma_{\mathrm{noise}} = 0.01$.

IV. Discussion

This Section discusses several advantages attendant to fitting the two-dimensional model of Eq. (1) to all data together, *i.e.*, single-step or integral processing. Repeating from the Introduction, Sec. I, they are

1) The number of free parameters to be estimated is strongly reduced with respect to two-step processing where the metabolite concentrations $\psi_m(t_n^{\mathrm{HP}})$ are to be estimated separately for each $n = 1, \ldots, 100$. This is deemed self-evident and will not be elaborated on.
   As for the number of free parameters, we have so far tacitly assumed that the nuclear precession frequencies are constant during the entire HP time span. Should frequency drift occur, measures as described in Ref. [20] are available.
2) In single-step processing, parameter estimates have smaller errors than in two-step processing.
3) Single-step processing can handle lower SNR's than does two-step processing.

A. *Single-step processing reduces errors*

Below, we treat the claimed error-reduction in the context of the standard MRS technique of *signal-averaging*.
Because the nuclear magnetic polarisation is tiny, MRS signals are weak. SNR enhancement by hyperpolarisation not yet being an obvious option [7], one usually resorts to measuring the signal not just once, but $N_{\mathrm{average}} \gg 1$ times, followed by averaging. This procedure increases the signal by N_{average}, but the noise only by $\sqrt{N_{\mathrm{average}}}$, resulting in an SNR enhancement by $\sqrt{N_{\mathrm{average}}}$.
In order to make the claimed error-reduction plausible, we invoke the following thought experiment. Instead of simply averaging repeated MRS signals prior to processing, one can leave them untouched and handle them all together in the same single-step manner as done for HP-MRS. The difference with HP-MRS data is that $\psi_m(t_n^{\mathrm{HP}})$ in Eq. (1) becomes the time-independent concentration c_m of metabolite species m. The task is now to establish the estimation errors corresponding to this approach. This is possible with CRB theory, using Eq. (11) and avoiding complicated algebra. Exploiting that the concentrations c_m are constant over time, the attendant Jacobian J' can be partitioned into N_{average} equal parts J'_{part}. It is important to note that J'_{part} is the Jacobian for each of the N_{average} measurements prior to adding. This leads to

$$J'^{\mathrm{T}}J' = N_{\mathrm{average}}\, J'^{\mathrm{T}}_{\mathrm{part}} J'_{\mathrm{part}}\,, \quad (12)$$

resulting in the CRB's

$$\mathrm{CRB}'_\ell = \frac{\sigma_{\mathrm{noise}}}{\sqrt{N_{\mathrm{average}}}} \sqrt{\left[(J'^{\mathrm{T}}_{\mathrm{part}} J'_{\mathrm{part}})^{-1}\right]_{\ell,\ell}}\,, \ell = 1, \ldots, L\,, \quad (13)$$

that can be seen to equal those pertaining to processing the averaged signal. This finding confirms that single-step processing of HP-MRS measurements is similar to averaging of repeated MRS measurements. It follows too that single-step processing can handle lower SNR's than two-step processing.

It should be pointed out that the above considerations enable one to improve two-step processing. This will be discussed in the next sub-Section.

B. *Extended two-step processing*

The content of this sub-Section is based on insight gained from the previous sub-Section.

Two-step processing of HP-MRS data can be improved significantly by introducing two extra steps prior to steps 1), 2), described in Sec.I. The extra steps are

a) First, one averages the MRS signals measured at t_n^{HP}, $n = 1, 2, \ldots, N^{\mathrm{HP}}$, which yields a single MRS signal with significantly enhanced SNR, in the same vein as with averaging in normal MRS.
b) Second, one estimates the concentrations, frequencies, and decay factors of the metabolites by NLLS-fitting of the model function of Eq. (6) to the single, averaged signal, yielding optimal values of the *non*linear parameters of type frequency and decay factor [8].

After a), b), estimation of the time-dependent concentrations of the various metabolite species $c_m(t_n^{\mathrm{HP}})$, *i.e.*, the original first step, is to be carried out. This task is now much easier because the nonlinear parameters are already known from step b). Hence, linear least-squares(LLS)-fitting rather than NLLS-fitting of Eq. (6) to N^{HP} MRS signals, is needed. This is advantageous because LLS-fitting is non-iterative and therefore

[7] The technique of hyperpolarisation is already commercially available, but is still expensive and complicated. In addition, steady-state hyperpolarisation of a patient's nuclei is a thing of the future.

[8] The average concentrations are estimated too but they have little use.

does not have a threshold-SNR below which it ceases to work optimally [9]. Consequently, extended two-step processing should enable to estimate concentrations from low-SNR MRS signals too.
Finally, the metabolite exchange constants k_m^1 are estimated, in step 2.
Summarising, extended two-step processing may yield the same final results as does single-step processing, but it is certainly more labour-intensive.

C. *Extended single-step processing*

The content of this sub-Section is based on insight gained from the previous two sub-Sections.

Single-step processing too can benefit from steps a), b), introduced in the previous sub-Section, at the cost of making it more labour-intensive. As above, step b) yields optimal values of the nonlinear MRS-parameters in Eq. (6). These values can be treated as known constants in the sequel. The advantage of this is that the number of free parameters in Eq. (10) can be more than halved, from 17 to 8, which in turn should ease the convergence of the attendant NLLS-fit. We emphasise that the latter NLLS-fit still involves all data-points, and that processing of all N^{HP} MRS signals individually is not done.

D. *Handling arbitrary in vivo MRS-signal decay*

For the sake of simplicity, we assumed basic exponential temporal decay $e^{-t/\tau_m^{\text{MRS}}}$ of the MRS-signal; see Subsec.II-C. This is justified when one merely wishes to prove the viability of single-step processing, in its simplest form. In *in vivo* experiments, the form of the decay is usually non-descript due to inhomogeneity of the magnetic field within a subject; see, *e.g.*, Ref. [5], specifically its Fig. 2 and attendant text. In spite of the arbitrariness of the decay, Ref. [5] simplified to either exponentional or Gaussian temporal decay. This gives rise to biased estimates [21]. We foresee that the form of the temporal decay can be estimated well from the averaged MRS-signal, obtained from step a) in Subsec. IV-B, using the method described in Proc. ICT.OPEN 2015, Ref. [15]. Insertion of the estimated decay as fixed entity in to the model function of Eq. (6) should reduce bias caused by *in vivo* conditions.

E. *Future research*

So far, our efforts were focused on developing and testing single-step processing of simulated HP-MRS data. Next, processing of real-world data, *e.g.*, those in Ref. [22] is to be investigated. Among other things, this will require proper estimation of the times t_a and t_e in Eqs. (2,3,4,5). In addition, multisite kinetic modelling [6] may need further development, using methods described in Ref. [23].

V. Concluding Remarks

This is a work in progress concerning a new approach to processing MRS measurements on magnetically hyperpolarised nuclei. So far, it turned out that the bias-to-standard deviation ratio's obtained from Monte Carlo experiments are small, while the standard deviations themselves agree well with the corresponding CRB's. We conclude that *processing all data together*, in a single step, and this directly in the measurement domain (= time domain),

1) is beneficial for the precision of estimated model parameters,
2) lowers the SNR that is tractable
3) is less labour-intensive than the traditional two-step approach mentioned in the Introduction.

[9] Each NLLS-fitting algorithm has a specific threshold SNR below which its performance starts to degrade.

Acknowledgements

This work was done in the context of FP7 - PEOPLE Marie Curie Initial Training Network Project PITN-GA-2012-316679-TRANSACT, http://www.transact-itn.eu/index.php, based in part on the free software package jMRUI, http://www.mrui.uab.es/mrui/.
DvO and RdB have been granted guest-status at the of Department of Imaging Physics, TNW, TUDelft.

Appendix 1

Details of the Jacobian matrix J, introduced in Subsec. II-D, indicating the chosen order of the sample times in the single step approach.

$$J = \begin{pmatrix} \frac{\partial s(t_1^{\text{HP}},t_1^{\text{NMR}})}{\partial p_1} & \frac{\partial s(t_1^{\text{HP}},t_1^{\text{NMR}})}{\partial p_2} & \cdots & \frac{\partial s(t_1^{\text{HP}},t_1^{\text{NMR}})}{\partial p_L} \\ \vdots & \vdots & & \vdots \\ \frac{\partial s(t_1^{\text{HP}},t_{N'}^{\text{NMR}})}{\partial p_1} & \frac{\partial s(t_1^{\text{HP}},t_{N'}^{\text{NMR}})}{\partial p_2} & \cdots & \frac{\partial s(t_1^{\text{HP}},t_{N'}^{\text{NMR}})}{\partial p_L} \\ \frac{\partial s(t_2^{\text{HP}},t_1^{\text{NMR}})}{\partial p_1} & \frac{\partial s(t_2^{\text{HP}},t_1^{\text{NMR}})}{\partial p_2} & \cdots & \frac{\partial s(t_2^{\text{HP}},t_1^{\text{NMR}})}{\partial p_L} \\ \vdots & \vdots & & \vdots \\ \frac{\partial s(t_2^{\text{HP}},t_{N'}^{\text{NMR}})}{\partial p_1} & \frac{\partial s(t_2^{\text{HP}},t_{N'}^{\text{NMR}})}{\partial p_2} & \cdots & \frac{\partial s(t_2^{\text{HP}},t_{N'}^{\text{NMR}})}{\partial p_L} \\ \vdots & \vdots & & \vdots \\ \vdots & \vdots & & \vdots \\ \frac{\partial s(t_N^{\text{HP}},t_1^{\text{NMR}})}{\partial p_1} & \frac{\partial s(t_N^{\text{HP}},t_1^{\text{NMR}})}{\partial p_2} & \cdots & \frac{\partial s(t_N^{\text{HP}},t_1^{\text{NMR}})}{\partial p_L} \\ \vdots & \vdots & & \vdots \\ \frac{\partial s(t_N^{\text{HP}},t_{N'}^{\text{NMR}})}{\partial p_1} & \frac{\partial s(t_N^{\text{HP}},t_{N'}^{\text{NMR}})}{\partial p_2} & \cdots & \frac{\partial s(t_N^{\text{HP}},t_{N'}^{\text{NMR}})}{\partial p_L} \end{pmatrix}$$

APPENDIX 2

Table II
TRUE VALUES, MEANS, ERRORS IN THE FITTED CHEMICAL EXCHANGE-PARAMETERS ESTIMATED BY A MONTE-CARLO PROCEDURE.

Exchange	Pyr→Lac	Pyr→Ala	Pyr→BC
True value	0.031940	0.025070	0.003790
Mean	0.031972	0.025075	0.003994
Bias	0.000032	0.000005	0.000204
Stdev	0.000853	0.000971	0.001110
CRB	0.000834	0.000957	0.001000

REFERENCES

[1] T.L. James, *Fundamentals of NMR*. http://qudev.ethz.ch/content/courses/phys4/studentspresentations/nmr/James_Fundamentals_of_NMR.pdf, 1998, ch. 1. 1

[2] E. Jobard, O.Tredan, D. Postoly F. Andre, A.L. Martin, B. Elena-Herrmann, S. Boyault, "A systematic evaluation of blood serum and plasma pre-analytics for metabolomics cohort studies," *International Journal of Molecular Sciences*, vol. 17, no. 12, p. 2035, Dec 2016. 1

[3] A.P. Siskos, P. Jain, W. Romisch-Margl, M. Bennet, D. Achaintre, Y. Asad, L. Marney, L. Richardson, A. Koulman, J.L. Griffin, F. Raynaud, F; A. Scalbert, A; J. Adamski, C. Prehn, H.C. Keun, , "Interlaboratory reproducibility of a targeted metabolomics platform for analysis of human serum and plasma," *Analytical Chemistry*, vol. 89, no. 1, pp. 656–665, Jan 2017. 1

[4] G. Jeschke and L. Frydman, "Nuclear hyperpolarization comes of age," *Journal of Magnetic Resonance*, vol. 264, pp. 1–2, 2016. 1

[5] M.A. Janich, M.I. Menzel, F. Wiesinger, E. Weidl, O. Khegai, J.H. Ardenkjaer-Larsen, S.J. Glaser and A. Haase, R.F. Schulte, and M. Schwaiger, "Effects of pyruvate dose on in vivo metabolism and quantification of hyperpolarized ^{13}C spectra," *NMR in Biomedicine*, vol. 25, pp. 142–151, 2012. 1, 2, 5

[6] P.A. Gómez Damián, J.I. Sperl, M.A. Janich, O. Khegai, F. Wiesinger, S.J. Glaser, Axel Haase, M. Schwaiger, R.F. Schulte, and M.I. Menzel, "Multisite Kinetic Modeling of ^{13}C Metabolic MR Using [1-^{13}C] Pyruvate," *Radiology Research and Practice*, vol. 2014, no. Article 871619, p. 10 pages, 2014, http://dx.doi.org/10.1155/2014/871619. 1, 2, 3, 5

[7] M. Karlsson, P.R. Jensen, J.H. Ardenkjaer-Larsen, and M.M. Lerche, "Difference between extra- and intracellular T-1 values of carboxylic acids affects the quantitative analysis of cellular kinetics by hyperpolarized NMR," *Angewandte Chemie - International Edition*, vol. 55, pp. 13 567–13 570, October 2016. 1

[8] C.H.Cunningham, J.Y.C. Lau, A.P. Chen, B.J. Geraghty, W.J. Perks, I. Roifman, G.A. Wright, and K.A. Connelly, "Hyperpolarized C-13 metabolic MRI of the human heart : Initial experience," *Circulation Research*, vol. 119, no. 11, pp. 1177–1182, November 2016. 1

[9] N. Nielsen, C. Laustsen, and L.B.Bertelsen, "C-13 dynamic nuclear polarization for measuring metabolic flux in endothelial progenitor cells," *Experimental Cell Research*, vol. 349, no. 1, pp. 95–100, November 2016. 1

[10] T.C. Salzillo, J. Hu, L. Nguyen, N. Whiting, J. Lee, J. Weygand, P Dutta, S. Pudakalakatti, N.Z. Millward, S.T. Gammon, F.F.Lang, A.B. Heimberger, and P.K. Bhattacharya, "Interrogating metabolism in brain cancer," *Magnetic Resonance Imaging Clinics Of North America*, vol. 24, no. 4, pp. 687–+, November 2016. 1

[11] J. Maidens, J.W. Gordon, M. Arcak, and P.E.Z. Larson, "Optimizing Flip Angles for Metabolic Rate Estimation in Hyperpolarized Carbon-13 MRI," *IEEE Transactions On Medical Imaging*, vol. 35, no. 11, pp. 2403–2412, November 2016. 1

[12] H. Nonaka, M. Hirano, Y. Imakura, Y. Takakusagi, K. Ichikawa, S. Sando, "Design of a ^{15}N molecular unit to achieve long retention of hyperpolarized spin state," *Scientific Reports*, vol. 7, p. 40104, Jan 2017. 1

[13] X. Ji, A. Bornet, B. Vuichoud, J. Milani, D. Gajan, A.J. Rossini, L. Emsley, G. Bodenhausen, S. Jannin, "Transportable hyperpolarized metabolites," *Nature Communications*, vol. 8, p. 13975, Jan 2017. 1

[14] D. van Ormondt, R. de Beer, A.J.H. Mariën, J.A. den Hollander, P.R. Luyten, and J.W.A.H. Vermeulen, "2D Approach to Quantitation of Inversion-Recovery Data," *Journal of Magnetic Resonance*, vol. 88, pp. 652–659, 1990. 1

[15] D. van Ormondt, R. de Beer, J.W.C. van der Veen, D.M. Sima, and D. Graveron-Demilly, "Improved estimation of the temporal decay function of in vivo metabolite signals," in *Proceedings ProRISC, ICT.OPEN 2015*. Amersfoort, The Netherlands: IPN, STW, NWO, 24-25 March 2015, pp. 36–41, http://www.ictopen2015.nl/content/Proceedings+2015. 2, 5

[16] D. Graveron-Demilly, "Quantification in Magnetic Resonance Spectroscopy Based on Semi-Parametric Approaches," *Magn. Reson. Mater. Phy.*, vol. 27, no. 2, pp. 113–130, April 2014. 2

[17] D. van Ormondt, D. Graveron-Demilly, D.M. Sima, S. Van Huffel, and S.R. Williams, *Time-Domain Methods for Quantifying MR Spectra*, ser. eMagRes. Wiley, 2015, vol. 4, ch. DOI10.1002/9780470034590.emrstm1427, pp. 651–662. 2

[18] D. Stefan, F. Di Cesare, A. Andrasescu, E. Popa, A. Lazariev, E. Vescovo, O. Strbak, S. Williams, Z. Starcuk, M. Cabanas, D. van Ormondt, and D. Graveron-Demilly, "Quantitation of magnetic resonance spectroscopy signals: The jMRUI software package," *Meas. Sci. Technol.*, vol. 20, 2009, http://iopscience.iop.org/0957-0233/20/10/104035/. 3

[19] L.L. Scharf and L.T. McWhorter, "Geometry of the Cramer-Rao bound," *Signal Processing*, vol. 31, pp. 301–311, 1993. 3

[20] J.W. van der Veen, S. Marenco, J. Shen, "Water sidebands removal in spectral fitting," in *Proc. 23rd Ann. Mtg. Intl. Soc. Mag. Reson. Med.*, vol. 23, Toronto, Ontario, Canada, 2015, p. 1970. 4

[21] D. van Ormondt, R. de Beer, D.M. Sima, and D. Graveron-Demilly, "Error-Bars in Semi-Parametric Estimation," in *ProRISC, ICT.OPEN*. Eindhoven, The Netherlands: IPN, STW, NWO, 27-28 November 2013, pp. 15–20, http://www.ictopen2013.nl/content/proceedings+2013. 5

[22] F. van Heijster, S. Heskamp, A. Veltien, T. Peeters, T. Scheenen, O. Boerman, A. Heerschap, "In vivo hyperpolarized [1-^{13}C]pyruvate and [^{18}F]-FDG PET/CT studies of prostate cancer metastasis xenografts in mice," in *Proceedings ISMRM-Benelux*, Tilburg, The Netherlands, 20 January 2017, pp. O–005. 5

[23] M. Holz and A. Fahr, "Compartment modeling," *Advanced Drug Delivery Reviews*, vol. 48, pp. 249–264, 2001. 5

2017-03-20, 14:02